OPEN ACCESS

UNIVERSITY OF DUNDEE

University of Dundee

Nondestructive Handheld Fourier Transform Infrared (FT-IR) Analysis of Spectroscopic Changes and Multivariate Modeling of Thermally Degraded Plain Portland Cement Concrete and its Slag and Fly Ash-Based Analogs

Leung Tang, Pik; Alqassim, Mohammad; Nic Daéid, Niamh; Berlouis, Leonard; Seelenbinder, John

Link to publication in Discovery Research Portal

Non-Destructive Handheld FTIR analysis of spectroscopic changes and multivariate modelling of thermally degraded plain Portland cement concrete and its slag and fly ash based analogues.

*Pik Leung Tang[A], Mohammad Alqassim[B,C], Niamh Nic Daéid[C], Leonard Berlouis[D], John Seelenbinder[E]

[A]Agilent Technologies UK Ltd, 5 Lochside Avenue, Edinburgh, UK. EH129DJ
*Corresponding author: leung_tang@agilent.com, m: +44790035539, f: +441314520600.
[B] General Department of Forensic Evidence and Criminology, Dubai Police GHQ, Dubai, UAE.
[C] University of Dundee, Dow St, Dundee, UK. DD15EH
[D] University of Strathclyde, 16 Richmond St, Glasgow, UK. G1 1XG
[E]Agilent Technologies, 14 Commerce Dr, Danbury, CT 06810

ABSTRACT:

Concrete is by far the world's most common construction material. Modern concrete is a mixture of industrial pozzolanic cement formulations and aggregate fillers. The former acts as the glue or binder in the final inorganic composite, however, when exposed to a fire the degree of concrete damage is often difficult to evaluate non-destructively. Fourier Transform Infrared (FTIR) spectroscopy through techniques such as transmission, attenuated total reflectance (ATR) and diffuse reflectance (DR) have been rarely used to evaluate thermally damaged concrete. In this paper, we report on a study assessing the thermal damage of concrete via the use of a non-destructive hand-held FTIR with a diffuse reflectance sample interface. *In situ* measurements can be made on actual damaged areas, without the need for sample preparation. Separate multivariate models were developed to determine the equivalent maximal temperature endured for three common industrial concrete formulations. The concrete mixtures were successfully modeled displaying high predictive power as well as good specificity. This has potential uses in forensic investigation and remediation services particularly for fires in buildings.

Index headings: Portable FTIR; diffuse reflectance; NDT/Non-destructive testing; Forensic

Investigation; blended concrete; thermal damage; heat treatment; PLS modelling; multivariate.

1. INTRODUCTION:

Portland cement[1] (PC) is by far the world's most widely used modern construction material. The importance of this material is manifested by the prevalence of cement organizations and societies[2, 3] based on national, continental, scientific, industry, consultancy and usage aspects. PC is mixed with suitable aggregates (fillers) and water to create a concrete, an inorganic composite. In addition, the cement may be blended with other pozzolanic materials such as ground granulated blast-furnace slag (GGBS) or Fly Ash (FA)[4-9] to achieve specific mechanical and/or chemical properties. The compressive strength of concrete is altered by thermal treatment[10, 11]; especially if the exposed heat is from an uncontrolled source such as a fire event[12]. Given the broad application of concrete and its susceptibility to thermal damage, there is interest in development of a non-destructive technique to evaluate the extent of thermal damage [13].

Thermal damage to concrete can cause a variety of chemical reactions including dehydration and carbonation. Additionally, solid-state transformation, solid-gas reactions and significant mass loss may occur. The majority of these reactions are observable using infrared spectroscopy[14, 15]. The chemical transformation of the base oxides and carbonates that constitute the raw precursor materials for PC production (lime, silica, alumina and iron oxide) requires a significant input of energy. To counter-balance the high energy costs, the base materials are both cheap and ubiquitous. Once the dry blended cement product is wet-mixed with the aggregate fillers and other additives they create a concrete mixture which cures in a very complex manner[2, 3], becoming a synthetic rock-like cross-linked heterogeneous material that is capable of carrying immense structural loads[9, 13, 16].

The four main hydraulically-active minerals in PC clinker are Alite, Belite, Celite and Ferrite[9, 17]. The first of these, Alite (tri-calcium silicate, >50% of PC) endows the binder of the concrete mixture with its early strength. Alongside this, a different and more slowly acting mineral, Belite

(di-calcium silicate, ~20% of PC) provides the concrete with its medium to long term strength. The final two minerals, Celite (tri-calcium aluminate) and Ferrite (tetra-calcium alumina ferrite) combined typically total up to about 20% of PC. They contribute very little to the final strength of the concrete. Their reaction mechanism requires the addition of a few percentage weight of gypsum in order to control and prevent false setting, *i.e.*, the latter two minerals cause premature and uncontrolled early solidification. Clearly, the majority of concrete components are inorganic but a very small fraction is organic or semi-organic, most commonly water reducing agents[18, 19]. The majority of the concrete ingredients absorb in the infrared region [19-21]. Therefore, any changes in their spectroscopic response can be directly linked to the chemical and physical state of the matrix. When hydrated, these changes can be analysed and modelled to reveal the degree of cure of the cement[20].

The purpose of this study is to demonstrate the feasibility of using a hand-held FTIR instrument in order to acquire the spectra from normal and thermally-treated concrete and to develop a model that could be correlated to residual compression strength. Three different cement mixtures were added to a common aggregate package resulting in three cured concrete types, namely A, B & C. These cured concrete samples were tested mechanically for their compressive strength and characterised using thermal analytical techniques in order to identify heating regimes that coincided with significant weight changes in the samples and therefore choose the most appropriate heat treatment regimes.

2. EXPERIMENTAL:

2.1 Concrete mixture design

Three concrete mixtures were prepared for the purpose of this study. The type of PC used was CEM I 42.5[22]. Mix A, which was considered as the control mixture, contained 100% PC as the binder material. In Mix B, GGBS was added as a 50% replacement of PC. Finally, for Mix C, FA

was added as a 20% replacement of PC. For all three concrete mixtures, the aggregate formed 78% of the total volume. All concrete mixtures were made using 0.4 free-water/cement ratio.

Table I gives the composition of the concrete mixtures used[21]. The admixture employed was a modern polycarboxylic ether-based super plasticiser[23] that reduces the water demand without detrimentally affecting the final material properties. Batches were mixed according to Table I and poured into moulds to create 100mm cubes conforming to British Standard European Norm (BS EN) 147-1.

Table I. Concrete Mix Design. Concrete Mix A contains 100% PC, Mix B contains 50% PC & 50% GGBS, Mix C contains 80% PC & 20% FA in their cement combinations. PC=Portland cement; GGBS=Ground Granulated Blast-furnace Slag; FA=Fly Ash.

MIX	Cementitious Materials kg/m^3			Water Content (L)	Aggregate^a kg/m^3				Ad-mixture (% of cement wt.)	Wet Density kg/m^3
	PC	GGBS	FA		10/20	4/10	0/4	0/0.6		
A	380	-	-	152	702	378	630	297	0.07	2541
B	190	190	-	152	695	375	626	294	0.07	2525
C	304	-	76	152	694	373	624	294	0.07	2520

^{a} Aggregate sizes are described using the designation d/D in millimetres, where d is the lower mesh size and D is the upper mesh size.

2.2 Instrumentation:

2.2.1 Fourier Transform Infrared (FTIR)

An Agilent Technologies 4300 Handheld FTIR[21] with a diffuse reflectance sample interface was used to acquire all the infrared spectra from the samples[24]. The diffuse reflectance sample interface imparts the infrared beam normal to the sample and collects the diffusely reflected light at a range of angles from 24 to 60 degrees from normal. The spectra were acquired by co-adding 128 scans for both the background and the sample at 8cm^{-1} resolution using Happ Genzel apodisation[25, 26]. The total collection time for each discrete spectra measurement was 40

seconds. All spectra were measured with a y axis scale of (-log(R/R_0); however, they are displayed using the mathematically equivalent absorbance notation. All samples were measured as-received with no additional sample preparation procedures. Data processing and multivariate modelling of infrared data were performed using Lab Cognition Panorama software package[27].

2.2.2 Thermogravimetric analysis(TGA)

The ball-milled concrete mixture powder samples, ~25mg, were analysed following various heat treatments using a Perkin Elmer model TGA7 thermogravimetric analyser coupled to a TAC7/DX controller[28]. The sample was heated from 40°C-900°C at a constant rate of 10°C /min under a flow rate of air at 30ml/min.

2.2.3 Mechanical Testing

For measuring the compressive strength gain with standard cure, 100 mm concrete cubes were tested in accordance with BS EN 12390-3 and reported as an average of the data from two samples. Each concrete cube was subjected to a constant loading rate of 0.7 ± 0.1 N/mm^2/s until failure. For compressive strength changes following thermal exposure, the 75 mm cubes were tested 24 hours after the heat treatment. Here, each cube sample was subjected to a constant loading rate of 0.24 N/mm^2/s until failure. The above noted standard does not specify a loading rate for this cube size but since these samples were thermally degraded, a lower compression rate was employed. Physical restrictions of the furnace have meant that the heat treatment samples were 25 mm smaller than the standard 100 mm cubes.

3. RESULTS & DISCUSSIONS:

3.1   Hand-held FTIR analysis of concrete components

The FTIR spectra of the main ingredients of concrete; viz. dune sand and gabbro (of three different mesh sizes), plus cement materials are shown in Figures 1 and 2. It is clear that they exhibit distinctive and unique spectral features. The aggregate mixture are present as an inert filler and reinforcement material that when used correctly in conjunction with the correct cement yields a concrete that can out-perform the cement itself.
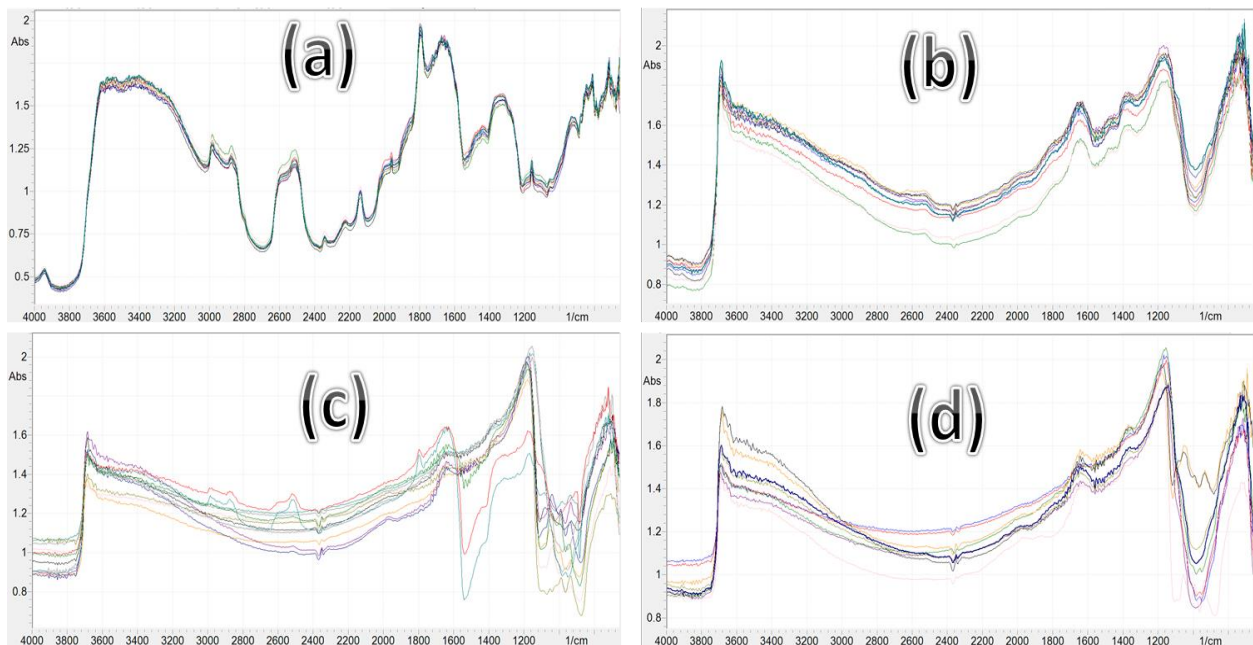

FIG **1. Handheld FTIR diffuse spectra of the aggregates common to all concrete mixtures: a) 0/0.6 dune sand, b) 0/4 gabbro, c) 4/10 crushed gabbro stone & d) 10/20 crushed gabbro stone. The non-uniformity in the spectra is evident in samples (c) and (d).**

The FTIR spectra of dune sand (Figure 1a) has absorption bands associated with carbonate and silicate as well as other minerals containing associated water, similar to some clay types[19, 20]. Specific absorbances are situated at 2500 cm^{-1} for the carbonate, from 1200 cm^{-1} to 900 cm^{-1} for the silicate and the broadband region beyond 3000 cm^{-1} for the hydrogen-bonded hydroxyl counter ion[29]. The fine dune sand was spectrally the most consistent in relation to the discrete

spectra taken at a wide variety of different sampling positions. The fine aggregate of 0/4 gabbro (Figure 1b) is a silicate-based mineral and appears to be fairly homogeneous with some spectra containing some minor carbonate. The two coarser grades of crushed gabbro stone at 4/10 (Figure 1c) and 10/20 (Figure 1d) of differ in that the 4-10mm mesh size occasionally contained carbonates with most the spectra similar to that of the fine aggregate (Figure 1b). The spectra of the coarse aggregates (Figures 1c and 1d) were more variable.

In the dune sand, there are not any sharp absorptions at ~3600-3750 cm^{-1} whereas these features are very commonly found in all clays [30] and indeed, in Figures 1(b), (c) and (d). These bulk aggregates do not react directly with the cementitious materials but on hydration of the alkaline cement mixture, to become an inter-connected network of cured cement and aggregate filler[31]. The cured PC chemically links with the surfaces of the aggregates[9]. The FTIR of the non-hydrated cementitious materials are shown in Figure 2, in order of decreasing pozzolanic activity, from PC > GGBS > FA[32]. For the PC sample, this contained the greatest amount and variety of complex associated and non-associated hydroxyl, as revealed in the region 3750 cm^{-1} to 2750 cm^{-1}. These hydroxyl species are found in smaller quantities and are much less diverse in the GGBS and FA samples[33, 34]. It can also be seen from the spectra that the amount of silicate decreases from GGBS to PC and FA, as depicted by the size of the negative Restrahlen peak at *ca.* 1100 cm^{-1}. Again, this silicate absorbance region is much more complex for the PC than for either the GGBS or FA materials. Also notable in the all three spectra is the existence of a peak at 1400-1500 cm^{-1} that has been tentatively assigned to alkali oxide possibly calcium oxide or other alkali metal.
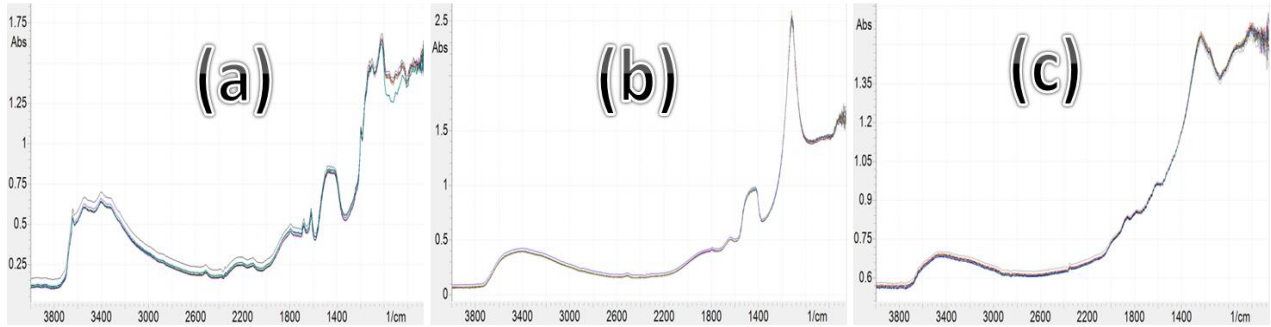
FIG 2. Handheld FTIR diffuse spectra of nominally pure and dry a) PC, b) GGBS and c) FA.

The FTIR spectra of the three cured concrete mixtures prepared from these materials appear quite similar in their raw spectra form, as shown in Figure 3a. However, the fine detail differences between the spectra can be highlighted by calculating the first derivative of the spectra (Figure 3b) and this reveals changes in both the free hydroxyl near 3625 cm^{-1} and bands due to silicate absorbance in from 1200 cm^{-1} to 800 cm^{-1}. This therefore suggests that concrete mixtures yield different products and so does not share exactly the same cure mechanisms due to the presence and reactivity of GGBS or FA in the concrete[35, 36].
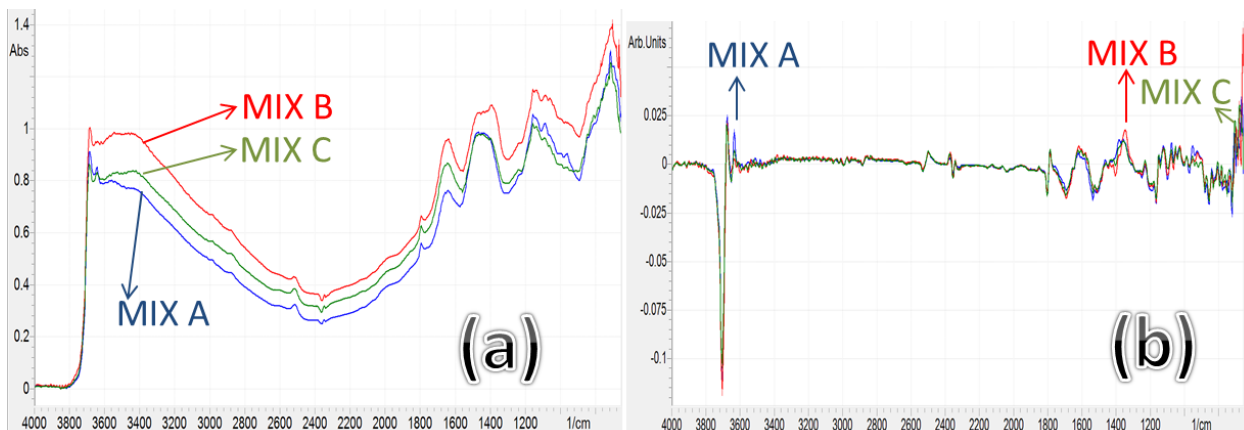

FIG 3. Diffuse FTIR spectra of:-a) Mix A, Mix B & Mix C diffuse spectra prior to thermal treatment, b) derivative of Mix A, B & C concrete.

3.2 Compressive strength and thermogravimetric analysis

The three concrete mixtures were found to increase their compressive strengths with standard

curing and this increased with ageing, as shown in Figure 4. These findings are noteworthy as they cover concrete with high compressive strength (Mix A), concrete for aggressive environments that may need sulphate, soil or sea-water resistance (Mix B) as well as a general purpose highly siliceous FA cement of medium strength[36] (Mix C). FA partial replacement of PC is frequently used to lower the carbon footprint and improve durability.
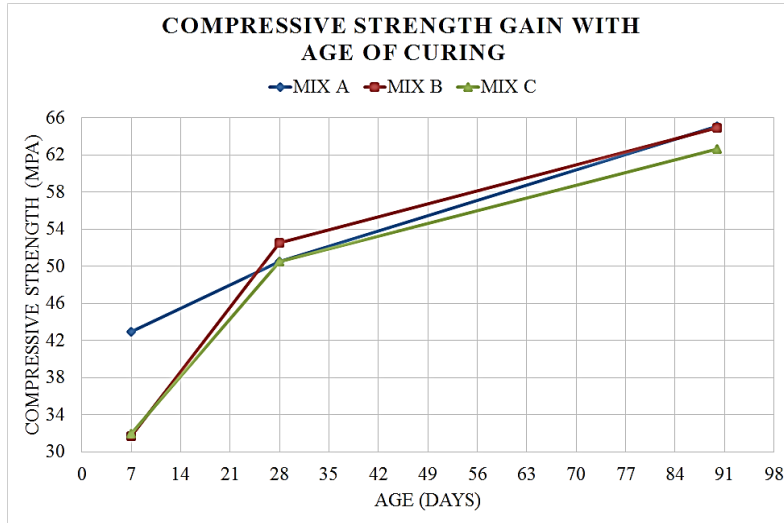

FIG 4. Compressive Strength (MPa) vs. Cure time (days) of Mix A, Mix B and Mix C (prior to heat treatment).

The use of the admixture has clearly enhanced the ultimate strength beyond the design target 28-day strength of 40 MPa for Mix A, 100% PC concrete mixture. More interestingly, the relatively low 7-day strengths of Mixes B and C catch up with that of the 100% PC of Mix A by 28 days and the strengths of the mixes increase in a remarkably similar manner beyond then. This data indicates that the three concrete mixtures surpassed the design strength by 17% by 90 days.

These concrete mixtures were initially analysed by thermogravimetric analysis (TGA) over the temperature range 40°C–900°C to obtain their mass loss profiles[28]. The three profiles are shown side-by-side to aid comparison in Figure 5. All three cured concrete mixtures exhibit a

slow dehydration between 40°C up to *ca.* 300°C but the amount of moisture lost is significantly different between the materials. The lowest water loss (~3 wt%) occurred in Mix A whereas Mix B and C both exhibited losses of *ca.* 5 wt%. A small (but not very distinct) weight loss event then occurs at between 300°C and 450°C, associated with breakdown of $Ca(OH)_2$. At *ca.*600° C, there was a sharp weight loss and this was due to the loss of CO_2 from the calcium carbonate. The amount lost here corresponded to *ca.* 7 wt%, 8 wt% and 10 wt% for Mix A, Mix B and Mix C, respectively. These three mixtures contain the same relative proportion of coarse and fine aggregates (Table I) which are the sources of carbonate. The major carbonate source by far though is the dune sand. The fact that different amounts of carbonate decomposition are revealed in the TGA thermograms of Mix A, Mix B and Mix C indicates that during curing, the high PC content of Mix A has reacted and reduced the amount of carbonate available for decomposition through a higher degree of cross-linking with the aggregates (Figure 1 & 2). Mix B has a reduced amount of pozzolanic activity due to its cementitious composition and so more of the carbonate can degrade. Mix C on the other hand contains FA particles that are of larger dimensions than GGBS and the ability to crosslink is therefore impeded, thus allowing more carbonate available for thermal decomposition.
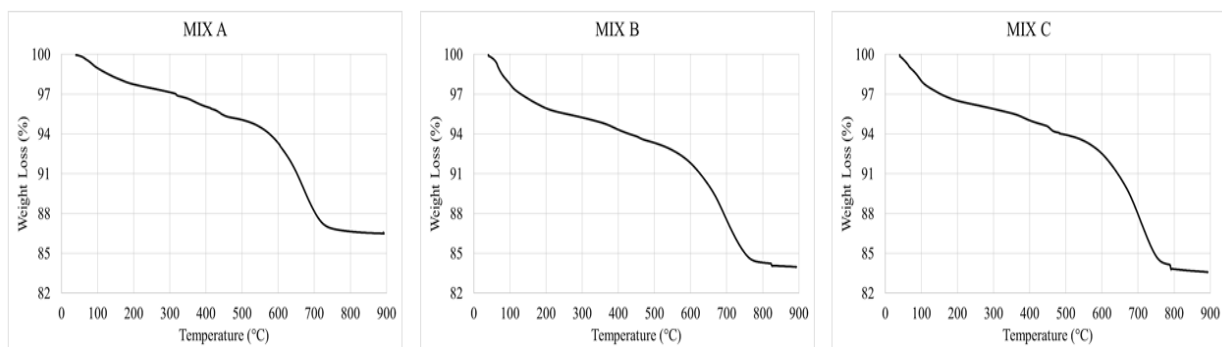

FIG 5. TGA profiles for Mixes A, B and C, ramp rate 10°C /min in Air

With the aid of the TGA data of Figure 5 and in combination with the known chemical

changes of concrete with temperature[10] and its behaviour in fires[37, 38] concrete mixtures A, B and C, were thermally degraded in a muffle furnace. The ramp rate of the furnace was 10°C/min to pre-determined temperatures of ambient (25°C), 150°C, 300°C, 600°C and 900°C. Each sample was kept at that set temperature for four hours and then allowed to cool naturally back to room temperature. The thermograms were collected for these treated samples and Figure 6 shows the data sets for each concrete mixture. Interestingly the weight loss profiles for the individual treatments showed a decrease in the number of temperature events with increasing treatment temperature. These changes in the thermograms are in agreement with the changes in the corresponding FTIR spectra.
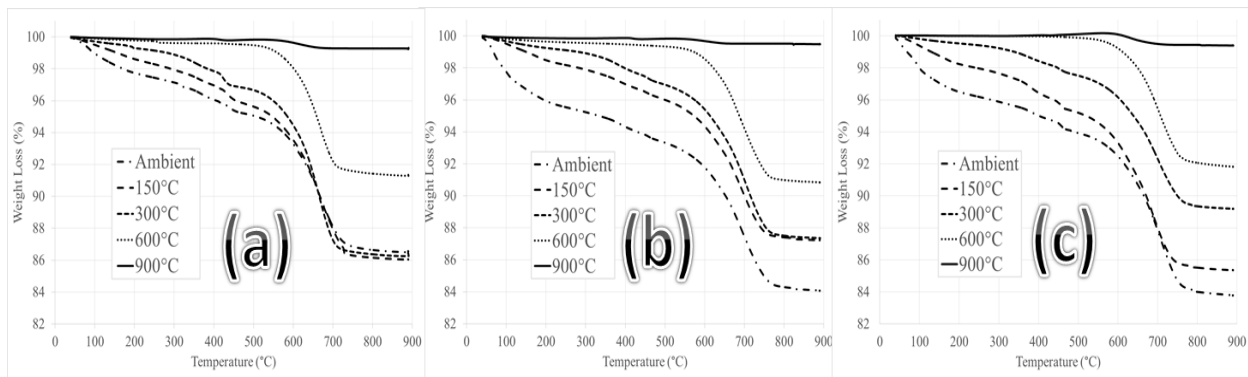

FIG 6. TGA profiles for Mixes A, B and C (a, b & c in figure, respectively) following different pre-treatments temperatures. TGA ramp rate 10°C /min in air.

The compressive strength changes following this thermal treatment are shown in Figure 7 for the three mixtures. At the moderate temperatures of *ca.* 25°C, 150°C and 300°C there was an actual increase in the compressive strength for two of the blended mixtures (Mix B & Mix C). This has been attributed to further post-cure of GGBS and FA which are less active at low temperatures[8]. For Mix A, the compressive strength fell slightly over this temperature range. Beyond 300°C however, all the samples suffered a decrease in compressive strength to 900°C.
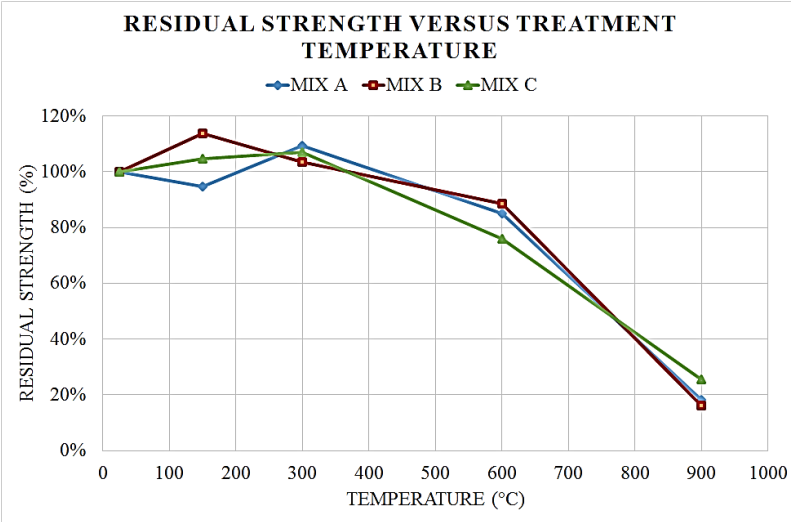
FIG 7. Residual strength of Mix A, B and C % with reference to their 90 day cure strength.

Changes in infrared spectra of the thermally treated samples are also observed as is shown in Figure 8. A decrease in the intensity of the broad, hydrogen bonded OH stretch band (3100 – 3600 cm^{-1}) is observed starting at 150 ° C; the decrease continues throughout the series of thermal treated samples. Additionally, two sharp bands are observed at ambient conditions arising from non-hydrogen bonded OH stretching at 3682 cm^{-1} and 3642 cm^{-1}; likely these two bands originate from isolated OH functional groups in different solid state conditions. As the thermal treatment is increased, the relative intensity of the band at 3642 cm^{-1} increases. This is likely due to a solid state transition occurring at higher temperatures. Infrared bands due to the absorbance of $CaCO_3$ at 2550 cm^{-1} and 1760 cm^{-1} appear to increase initially, then completely disappear in the final sample exposed to 900° C. The increase is relative and primarily a result of the overall sample dehydration. The reduction at 900° C corresponds to the thermal degradation of $CaCO_3$ that begins at 600° C and is fully degraded by 850° C[39]. In addition to the changes in carbonate and hydroxyl, changes are observed in the silicate absorbance bands in the region from 1200 – 800 cm^{-1}.
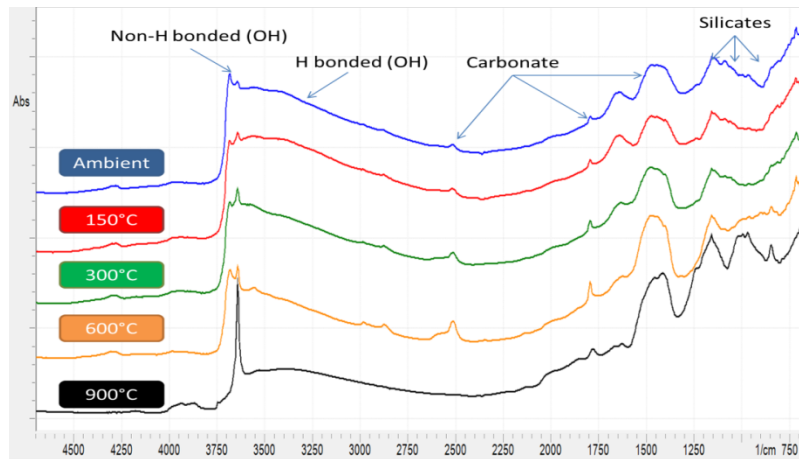
Figure 8: Average diffuse FTIR spectra following each heat treatment for concrete Mix A, showing thermal treatment related changes in relative absorbance of bands arising from non-hydrogent bonded OH, hydrogen bonded OH, carbonates and silicates.

3.3 Multivariate analysis

Multivariate models were developed correlating the FTIR spectra collected to the exposure temperature of the thermally treated concrete samples. A separate model was created for each concrete type, incorporating 40 calibration spectra. Each model was evaluated using a separate validation set of 10 spectra. The representative calibration FTIR spectra obtained at ambient, 150°C, 300°C, 600°C and 900°C are shown in Figures 9a, 10a and 11a for Mix A, Mix B and Mix C respectively. The actual versus predicted plot from each of the models employed are likewise shown in Figures 9b, 10b and 11b. All the models used the same pre-processing procedure, *viz.* mean-centred and Savitsky-Golay first derivative using nine points and a 3rd order polynomial. The model for Mix A used three factors over the selected regions of 3773–3520 cm^{-1}, 3025–2015 cm^{-1} and 1845–800 cm^{-1}. This model generated a root mean standard error of cross validation (RMSECV) of 16.9°C and an actual versus predicted linear fit of R^2 = 0.997. The model for Mix B used 2 factors over the selected regions of 3855–3505 cm^{-1}, 2592–2390 cm^{-1} and 1845–800 cm^{-1}. This model generated a root mean standard error of cross validation (RMSECV) of 12.6°C and an actual versus predicted linear fit of R^2 = 0.998.

Finally, that for Mix C used two factors over the selected regions of 3896–3440 cm^{-1}, 2626–2173 cm^{-1} and 1845–800 cm^{-1}. This model generated a root mean standard error of cross validation (RMSECV) of 25.5 degrees and an actual versus predicted linear fit of $R^2 = 0.994$.

FIG 9. a) Average diffuse FTIR spectra following each heat treatment for concrete Mix A, b) Actual vs. Predicted plot derived from multivariate PLS model for Mix A using 40 discrete spectra & 10 validation spectra

FIG 10. a) Average diffuse FTIR spectra following each heat treatment for concrete Mix B, b) Actual vs. Predicted plot derived from multivariate PLS model for Mix B using 40 discrete spectra & 10 validation spectra
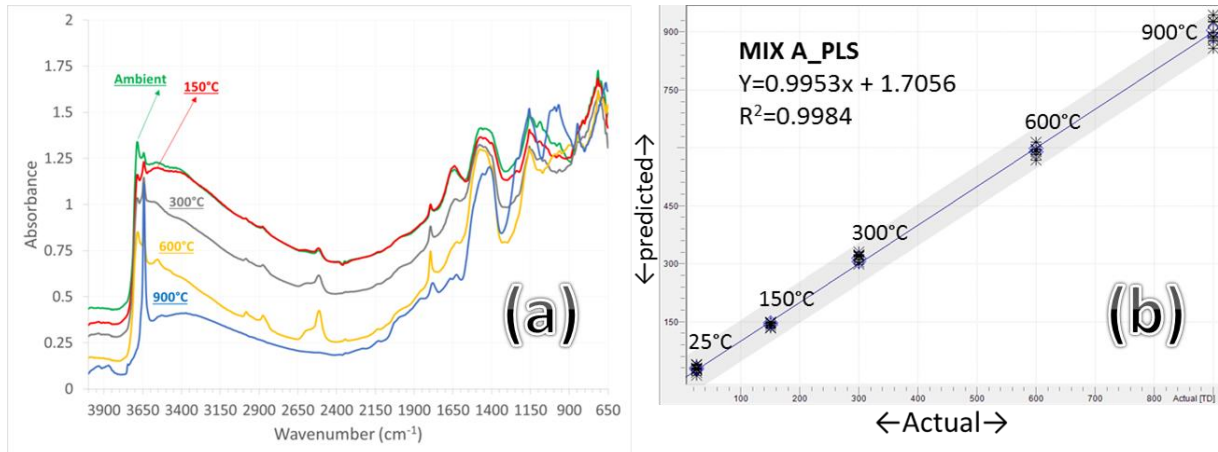
FIG 11. Average diffuse FTIR spectra following each heat treatment for concrete Mix C, b) Actual vs. Predicted plot derived from multivariate PLS model for Mix C using 40 discrete spectra & 10 validation spectra.
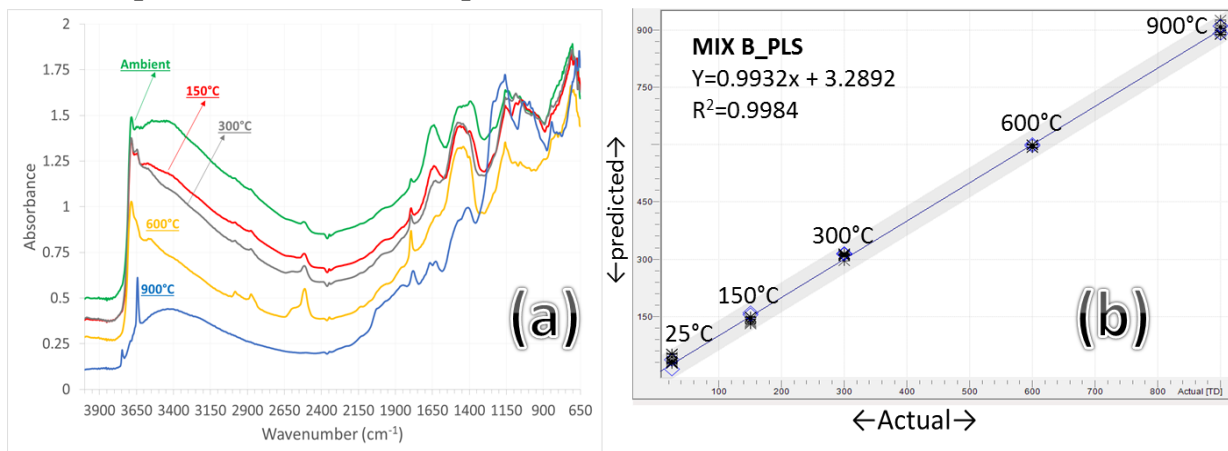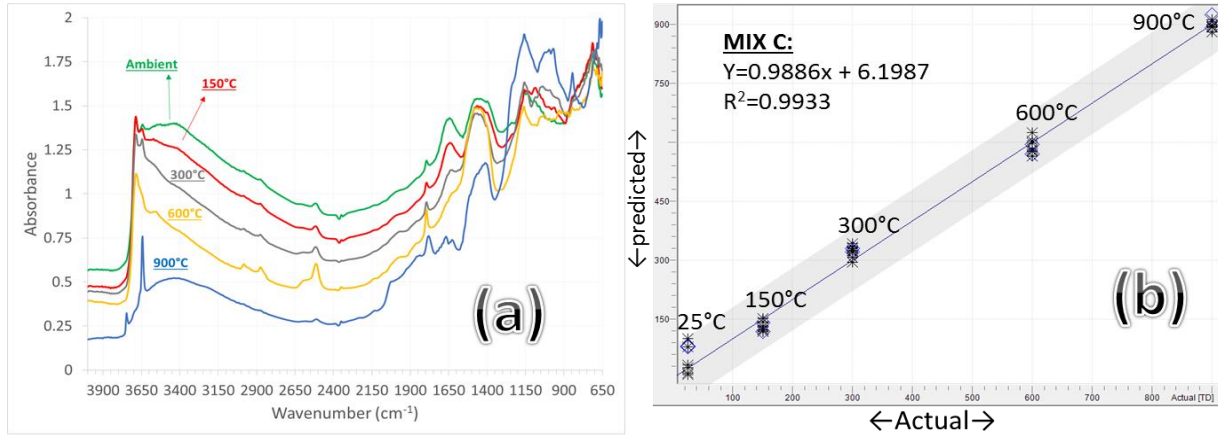
Although each of the models could predict the exposure temperature in very good agreement with the actual one employed, clearly Mix C was the most difficult since this one had nearly twice the RMSECV of the other two mixes. Also the actual versus predicted plot for this mixture showed poor correlation for the room temperature and 150°C samples. Relatively small changes are observed in the infrared spectra, TGA data and residual strength data in this temperature range for Mix C. Small changes can be difficult to model, especially when the total range of temperatures measured was so large. The three models were tested with 10 validation spectra each, *viz.* 2 samples from each of the 5 different temperature conditions. The full results of the individual validation sets are listed in Table IV.

Table IV. Validation results for PLS models predicting temperature exposure for Mix A, B and C.

Actual /°C	Predicted Validation Set/°C					
	Mix A		Mix B		Mix C	
25	27.6	31.2	12.6	37.7	78.5	80.7
150	147.8	143.2	154.5	159.8	141.4	118.1
300	314.9	304.8	315.6	313.7	320.5	330.8
600	588.5	597.9	601.4	597	597	569
900	890.9	905.1	909.4	890.8	892.1	925.1
RMSEP	7.66°C		10.23°C		31.76°C	

As with the cross validation results, both Mix A and Mix B show good exposure temperature predictions across the entire range of test samples, with root mean standard error of prediction (RMSEP) of 7.66°C and 10.23°C, respectively. As noted above, the prediction for the Mix C samples are poor at the lower temperature values of 25°C and 150°C and this contributes to the higher RMSEP of 31.76°C Although the model for Mix C does not perform as well as those for the other two mixtures, it is nevertheless sufficiently accurate to use for establishing the thermal exposure of FA containing concretes given that the significant attenuation in residual strength occurs between 300°C and 600°C[40]. Furthermore, all three models give excellent prediction for the higher temperature treatments between 600°C-900°C where the residual strength of all three concrete types fall steeply.

4. CONCLUSIONS:

The aim of this study has been to develop a method of establishing the thermal history of concrete structures through the use a handheld FTIR instrument with a diffuse reflectance sample interface. The results have demonstrated the development of a model using multivariate data analysis, for the non-destructive evaluation of thermally damaged and degraded specimens. Three successful multivariate methods were developed for three different concrete formulations that are typically deployed for specific civil engineering applications. These models show good potential which could be further extended to other types of concrete. The handheld FTIR instrument could provide accurate non-destructive testing of thermal degradation and lead to fast and efficient mapping of fire damage.

5. REFERENCES:

1. Lechtenberg, M., *Top 20 global cement companies*, in *Global Cement Magazine*. December 2012, Pro Publication International Ltd.: Epsom, UK.
2. Kosmatka, S.H., W.C. Panarese, and P.C. Association, *Design and control of concrete mixtures*. 2002.
3. Naik, T.R., *Sustainability of concrete construction*. Practice Periodical on Structural Design and Construction, 2008. **13**(2): p. 98-103.
4. Rozière, E., et al., *Durability of concrete exposed to leaching and external sulphate attacks*. Cement and Concrete Research, 2009. **39**(12): p. 1188-1198.
5. Berndt, M., *Properties of sustainable concrete containing fly ash, slag and recycled concrete aggregate*. Construction and Building Materials, 2009. **23**(7): p. 2606-2613.
6. Naik, T.R. and R. Kumar, *Sustainable Concrete with Industrial and Postconsumer By-Product Materials*. Green Building with Concrete: Sustainable Design and Construction, 2015: p. 337.
7. Pacheco-Torgal, F., J. Castro-Gomes, and S. Jalali, *Alkali-activated binders: A review: Part 1. Historical background, terminology, reaction mechanisms and hydration products*. Construction and Building Materials, 2008. **22**(7): p. 1305-1314.
8. Fitos, M., et al., *Pozzolanic activity of thermally and mechanically treated kaolins of hydrothermal origin*. Applied Clay Science, 2015. **116**: p. 182-192.
9. Taylor, H.F., *Cement chemistry*. 1997: Thomas Telford.
10. Willam, K., I. Rhee, and Y. Xi, *Thermal degradation of heterogeneous concrete materials*. Journal of materials in civil engineering, 2005. **17**(3): p. 276-285.
11. Poon, C.-S., et al., *Comparison of the strength and durability performance of normal-and high-strength pozzolanic concretes at elevated temperatures*. Cement and Concrete Research, 2001. **31**(9): p. 1291-1300.
12. Schneider, U., *Concrete at high temperatures—a general review*. Fire safety journal, 1988. **13**(1): p. 55-68.
13. Schneider dos Santos, R., S.B.A. Rolim, and F. Hepp Pulgati, *Application of visible and near infrared spectroscopy in non-destructive evaluation of cement materials*. International Journal of Remote Sensing, 2015. **36**(3): p. 917-938.

14. Ylmén, R., et al., *Early hydration and setting of Portland cement monitored by IR, SEM and Vicat techniques*. Cement and Concrete Research, 2009. **39**(5): p. 433-439.
15. Yut, I. and A. Zofka, *Fingerprinting of Chemical Admixtures in Fresh Portland Cement Concrete by Portable Infrared Spectrometer*. Transportation Research Record: Journal of the Transportation Research Board, 2012(2290): p. 1-9.
16. Pratt, P., et al., *Electron microscope studies of Portland cement microstructures during setting and hardening [and discussion]*. Philosophical Transactions of the Royal Society of London A: Mathematical, Physical and Engineering Sciences, 1983. **310**(1511): p. 93-103.
17. Barron, A.R., *Hydration of Portland Cement*. Connexions Project, 2010.
18. Chollet, M. and M. Horgnies, *Analyses of the surfaces of concrete by Raman and FT‑IR spectroscopies: comparative study of hardened samples after demoulding and after organic post‑treatment*. Surface and Interface Analysis, 2011. **43**(3): p. 714-725.
19. Nyquist, R.A. and R.O. Kagel, *Handbook of infrared and raman spectra of inorganic*

compounds and organic salts: infrared spectra of inorganic compounds. Vol. 4. 2012: Academic press.

20.   Fernández-Carrasco, L., et al., *Infrared spectroscopy in the analysis of building and construction materials*. 2012: INTECH Open Access Publisher.

21.   Rein, A., Higgins, F., *Use of Handheld FTIR for Elucidating Rock and Mineral composition*, in *Agilent Technologies application note*. 2011.

22.   BS EN, *197-1: 2011.* British Standard. Part I: Composition, Specifications and Conformity Criteria for Common Cements, 2011.

23.   BASF, *MasterGlenium® 51*, in *Polycarboxylic ether based, high range super plasticising admixture for concrete*, E.-T. ASTM C494 type F, IS 9103, Editor. 1999.

24.   Accardo, G., et al., *Diffuse Reflectance Infrared Fourier Transform Spectroscopy for the Determination of Asbestos Species in Bulk Building Materials.* Materials, 2014. **7**(1): p. 457-470.

25.   Codding, E.G. and G. Horlick, *Apodization and phase information in Fourier transform spectroscopy.* Applied Spectroscopy, 1973. **27**(2): p. 85-92.

26.   Bretzlaff, R. and T. Bahder, *Apodization effects in Fourier transform infrared difference spectra.* Revue de physique appliquée, 1986. **21**(12): p. 833-844.

27.   LabCognition, *Panorama*. 2008.

28.   Inc., P. *Pyris 1 TGA*. 2016 [cited 15 Jan. 2016]; Available from: http://www.perkinelmer.co.uk/Catalog/Product/ID/N5370742.

29.   Ebbert, C., et al., *Toward a microscopic understanding of the calcium–silicate–hydrates/water interface.* Applied Surface Science, 2014. **290**: p. 207-214.

30.   Madejová, J., *FTIR techniques in clay mineral studies.* Vibrational spectroscopy, 2003. **31**(1): p. 1-10.

31.   Nasrazadani, S. and T. Springfield, *Application of Fourier transform infrared spectroscopy in cement Alkali quantification.* Materials and Structures, 2014. **47**(10): p. 1607-1615.

32.   Pacewska, B. and I. Wilińska, *Comparative investigations of influence of chemical admixtures on pozzolanic and hydraulic activities of fly ash with the use of thermal analysis and infrared spectroscopy.* Journal of Thermal Analysis and Calorimetry, 2015. **120**(1): p. 119-127.

33.   Saafi, M., et al., *Enhanced properties of graphene/fly ash geopolymeric composite cement.* Cement and Concrete Research, 2015. **67**: p. 292-299.

34.   Dung, N.T., T.-P. Chang, and C.-T. Chen, *Hydration process and compressive strength of slag-CFBC fly ash materials without Portland cement.* Journal of Materials in Civil Engineering, 2014.

35.   Al Bakri, A.M., et al., *Mechanism and Chemical Reaction of Fly Ash Geopolymer Cement-A Review.* Journal of Asian Scientific Research, 2011. **1**(5): p. 247-253.

36.   Kocak, Y. and S. Nas, *The effect of using fly ash on the strength and hydration characteristics of blended cements.* Construction and Building Materials, 2014. **73**: p. 25-32.

37.   Fristom, R., *Flame structure and processes*. 1995: Oxford University Press.

38.   Harper, C.A., *Handbook of building materials for fire protection*. 2003: McGraw Hill Professional.

39.   Rodriguez-Navarro, C., et al., *Thermal decomposition of calcite: Mechanisms of formation and textural evolution of CaO nanocrystals.* American Mineralogist, 2009.

94(4): p. 578-593.

40.   Hussin, M., et al., *Performance of blended ash geopolymer concrete at elevated temperatures.* Materials and Structures, 2014. **48**(3): p. 709-720.